Research Article

Sevinch Rahimi Moghaddam, Bora Derin*, Onuralp Yucel, M. Seref Sonmez, Meltem Sezen, Feray Bakan, Vladimir N Sanin, and Dimitriy E Andreev

Production of Mo_2NiB_2 Based Hard Alloys by Self-Propagating High-Temperature Synthesis

https://doi.org/10.1515/htmp-2019-0020
Received Oct 11, 2017; accepted Feb 26, 2019

Abstract: Mo-Ni-B-Al as-cast alloys containing 35.5-58.7 wt% Mo, 23.0-57.6 wt% Ni, 3.3-5.2 wt% B, and 2.2-13.5 wt% Al were synthesized by Self-Propagating High-Temperature Synthesis (SHS) using a mixture of MoO_3, NiO, B_2O_3 and Al powders in order to obtain low-cost Mo_2NiB_2 containing hard materials. The first series of experiments were performed using 1.05 times the stoichiometric amount of Al. In the second series of experiments, FactSage thermochemical modeling software was used to minimize Al increasing the Mo_2NiB_2 formation in the as-cast alloys. The products were characterized by using atomic absorption spectrometry (AAS), X-ray diffraction (XRD), scanning electron microscopy (SEM) and microhardness techniques.

Keywords: Hard materials; Mo_2NiB_2; SHS; XRD; SEM

1 Introduction

Hard alloys are used in a broad range of applications due to their excellent properties such as high hardness and wear resistance as well as high toughness. The hard alloys based on wolfram carbide are the most widely used in various industrial areas [1]. However, due to the rare and uneven distribution of tungsten resources, some recent studies have focused on finding alternative hard materials with less or no tungsten in composition [2].

Transition metal borides are known for their unique physical, chemical and mechanical properties such as good refractoriness, chemical inertness, high hardness, and metallic conductivity. Among the ternary boride compounds reported in Mo-Ni-B system, Mo_2NiB_2 is the promising candidate for the reinforcement phase of the boride base cermets in wear resistant applications [3, 4]. Mo_2NiB_2 possesses orthorhombic crystal structure, with a Vickers hardness of 1500-2000 HV. It was found that the addition of 10-15 wt% Cr into the ternary compound imparts high elastic modulus that is comparable to that of tungsten carbides [2]. Because of the above-mentioned properties and excellent corrosion resistance, the hard alloys containing Mo_2NiB_2 have already been applied for plastic injection molding machine parts, cutters for heat sealers, drills for sand molds, etc. [4, 5].

There are some reported studies on the Mo_2NiB_2 containing hard alloys in the literature. For example, Takagi *et al.* synthesized the hard alloys consisting of Mo_2NiB_2 complex boride as a reinforcement phase and metallic Ni as a binder using reaction boronizing sintering method [6–9]. In their study, these hard materials were formed by in-situ liquid phase reactions starting from pure elements or high purity alloy powders. They claimed that the initial Mo/B ratio has an influence on the formation of complex borides [5]. Moreover, they found that the addition of different alloying elements to these ternary hard alloys changes the boride structure that causes remarkable improvements in mechanical properties [9]. In their another study, they proved that Mo_2NiB_2+Ni two-phase hard alloys causes significant improvements such as high transverse rupture strength (1.7 GPa), high fracture toughness and also superior corrosion resistance in contact with molten fluorocarbon resin [10]. However, this production method has some drawbacks such as high energy consumption, expensive raw materials, and difficulties in large-scale productions. Therefore, choosing an inexpensive production method for these hard materials to increase their abundance and their usage in wider range of applications has great importance.

***Corresponding Author: Bora Derin:** Metallurgical and Materials Engineering Department, Istanbul Technical University, Maslak, Istanbul, Turkey; Email: bderin@itu.edu.tr
Sevinch Rahimi Moghaddam, Onuralp Yucel, M. Seref Sonmez: Metallurgical and Materials Engineering Department, Istanbul Technical University, Maslak, Istanbul, Turkey
Meltem Sezen, Feray Bakan: Nanotechnology Research and Application Center, Sabancı University, Istanbul, Turkey
Vladimir N Sanin, Dimitriy E Andreev: Institute of Structural Macrokinetics and Materials Science, Russian Academy of Sciences, Chernogolovka, Moscow, Russia

Table 1: The amounts of the initial raw materials amount used in the experiments

Series of Exp	Exp No	MoO_3	NiO	B_2O_3	Al	Times the stoich. Al amount
		Weight, g				
1	Sample A	58.7	22.8	18.5	41.8	1.05
	Sample B	57.3	28.9	13.8	39.1	1.05
	Sample C	54.6	32.2	13.2	38.4	1.05
2	Sample D	46.9	28.1	25.0	35.0	0.80
	Sample E	41.0	34.4	24.6	34.2	0.80
	Sample F	28.6	42.9	28.6	30.3	0.70

The self-propagating high temperature synthesis method (SHS) is a self-sustained combustion process that is used in the production of many different advanced materials. SHS methods provide various advantages such as short process time and low energy consumption that make them suitable for the production of different materials including boride based ceramics [11], intermetallic compounds [12], binary or ternary alloys [13], heat resistant refractory materials [14] etc. The thermite-type SHS processes, which have highly exothermic reduction-oxidation reactions, were used in many industrial applications [16–18]. Recently, the SHS method was used for the production of the as-cast Mo_2NiB_2-Ni metal matrix composites by using a centrifugal machine. Sanin *et al.* used metallic oxides and elemental boron as the raw materials for the aluminothermic-SHS reaction under the acceleration values *(a)* ranging from 1 to 100 *g* (*g*: gravity) [19]. They concluded that the yield of the alloy products increases to nearly 100% by increasing *a/g*. Nevertheless, the product capacity, time and energy consumptions are the limitations in the use of centrifugal machines for the SHS processes.

Therefore, the present work aimed the production of hard alloys containing complex borides by using simple and low cost SHS method under earth-gravity (1 *g*) and ambient conditions. The mixtures of MoO_3, NiO, B_2O_3 and Al powders with different ratios were used as the raw materials. Also utilizing FactSage simulations [20], the thermodynamical mechanisms of simultaneous formations of the nickel-based solid solutions and boride compounds in Mo-Ni-B-Al systems were investigated.

2 Experimental Studies

In the SHS experiments, MoO_3 (Alfa Aesar, 99.5% pure, particle size <60 μm), NiO (99% pure, particle size<40 μm), B_2O_3 (98% pure, particle size<20 μm), Al (99.7% pure, particle size <60 μm) powders were used as starting materials. B_2O_3 was obtained by the calcination of pure boric acid (Eti Holding Inc. 99.5% pure) in a nickel crucible at 800°C for 2h. The powders with different ratios were prepared and then were dried in an oven at 105°C for 30 minutes. After thoroughly mixing of powders in the turbula mixer, about 140 g of the mixture was placed into a copper crucible with a height of 140 mm and an internal diameter of 50 mm and a wall thickness of 5 mm. Due to the release of high amounts of gases during the aluminothermic process, the experiments were performed in open crucibles under air. A tungsten filament on top of the powder mixture which is connected to a power supply initiated the exothermic reaction. After the SHS process, the alloy part was separated from slag and then was metallographically prepared for further analysis. The compositions of the initial reaction mixtures used in the experiments were presented in Table 1. The first series of experiments were performed using 1.05 times the stoichiometric amount of Al to achieve full reduction of the different initial oxide mixture. In the second series experiments, the compositions in the initial mixtures were determined by FactSage thermochemical modeling software [20] to minimize Al content, increasing the Mo_2NiB_2 formation in the as-cast alloys.

The crystal structure and the phases of the final products were determined by X-ray diffraction measurements (XRD, PANalytical PW3040/60 with a Cu-Kα radiation). The microstructure, morphology and the composition of phases were characterized by scanning electron microscopy equipped with an energy dispersive spectroscopy (SEM/EDS, Jeol JSM-840) and ImageJ® image analysis software. The elements were analyzed by atomic absorption spectrometer (AAS, Perkin-Elmer 1100B). The Vickers hardness test (Shimadzu Corporation HMV) with 5N indentation load was also carried out on the specimens.

Table 2: The stoichiometrically calculated and actual elemental compositions of the as-cast alloys from the first series of experiments

Exp No	wt%						
	Stoich. Calculated Compositions			Actual Compositions			
	Mo	Ni	B	Mo	Ni	B	Al
A	62.1	28.8	9.11	58.7	23.01	5.22	12.48
B	58.5	34.9	6.6	55	25.55	4.06	13.5
C	54.9	38.9	6.2	52.9	32.04	3.93	8.36

Table 3: The EDS measured elemental compositions for crystalline phases shown in Figures 1(a), (b), and (c)

	wt%					
	No	Mo	Ni	B	Al	Phase
Figure 1(a)	1	1.30	67.91	-	30.79	β-NiAl
	2	88.57	1.38	10.05	-	MoB
	3	83.31	-	16.69	-	MoB_2
	4	78.55	1.61	19.84	-	MoB_2
	5	79.04	1.73	19.23	-	MoB_2
Figure 1(b)	1	-	68.95	-	31.05	β-NiAl
	2	53.95	20.45	19.39	6.21	Mo_2NiB_2
	3	2.53	68.41	-	29.06	β-NiAl
	4	84.72	2.41	12.87	-	MoB_2
	5	81.64	3.67	14.69	-	MoB_2
Figure 1(c)	1	4.29	74.34	-	21.37	β-NiAl
	2	70.10	16.14	13.76	-	Mo_2NiB_2
	3	84.98	3.55	11.47	-	MoB

3 Results and Discussion

The stoichiometrically calculated compositions and the chemical analysis results of the as-cast alloys from the first series of experiments obtained by AAS are shown in Table 2. The obtained results revealed that the actual alloy compositions are different from the calculated ones due to the high amount of Al in the alloys and above-mentioned SHS nature. The aluminum content in the samples varied from 8.36 to 13.05 wt%, whereas boron content changed between 3.93 and 5.22 wt%. The Mo/Ni weight percent ratios in the obtained samples were detected to be between 2.55 and 1.65.

The backscattered electron (SEM/BSE) images of the as-cast alloys obtained by 1.05 times the stoichiometric amount of Al are shown in Figure 1(a-c). The elemental distributions of the phases in as-cast alloys revealed by Energy Dispersive Spectroscopy (EDS) scans are listed in Table 3. The results show that all samples are intermetallic matrix composites (IMCs). The common matrix in the samples was detected as beta (NiAl) nickel aluminide intermetallic phase which is a consequence of high Al content in the initial reactant mixture. Among the alloys studied in this work, sample A has the highest Mo content (58.7 wt%). Figure 1a and EDS scans prove that the molybdenum diboride (MoB_2) and molybdenum mono boride (MoB) are the two reinforcement phases in sample A. As seen in Figure 1b and 1c, when the nickel contents in the alloys increases, besides the matrix phase, Ni also tends to react with Mo and B to form a Mo_2NiB_2 ternary phase (light gray). Figure 1c also confirms that the Mo_2NiB_2 content increases with decreasing Al concentration in the alloy. The area fractions of distributed particles and overall matrix were measured by image analysis method from the SEM images using ×500 magnification. The reinforcement/matrix ratio for alloys A, B and C were found to be 0.92, 0.69 and 1.04, respectively, in rather good agreement with the measured alloy composition. In fact alloy B, which has low Mo content and high residual aluminum, show the lowest reinforcement/matrix ratio.

Before the second series of the experiments, some additional thermochemical calculations were employed to describe the phase transformations occurring during the SHS process and the solidification. The modeling was performed by using the advanced "Equilib" module of

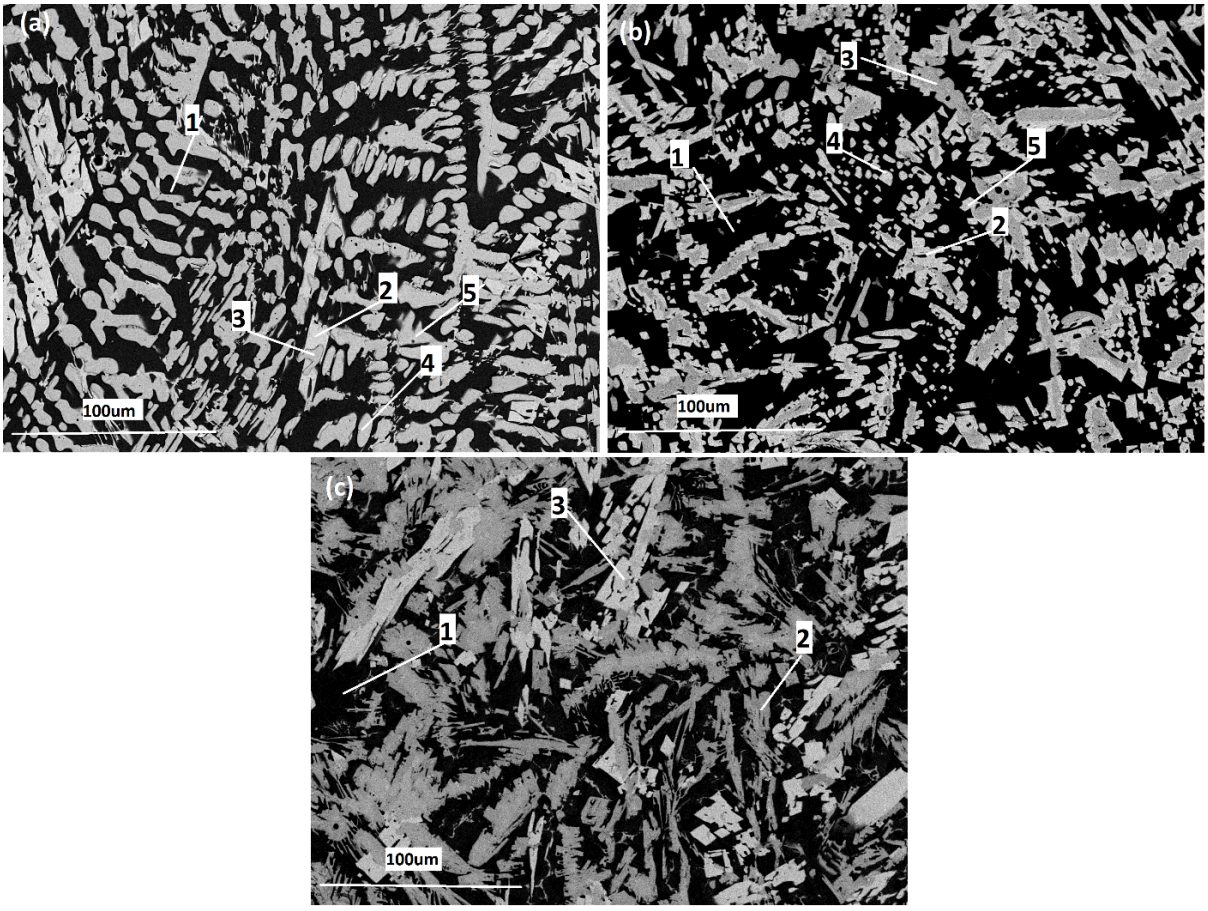

Figure 1: SEM/BSE images of the as-cast alloys from the first series of experiments (×500) a) Sample A, b) Sample B, and c) Sample C.

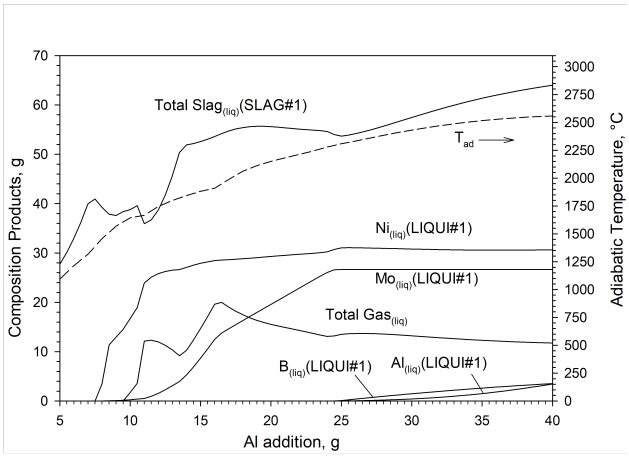

Figure 2: Selected phases and T_{ad} values of an SHS process versus Al by FactSage Calculation (40 g MoO_3+40 g NiO + 20 g B_2O_3+ <5-40> g Al)

FactSage 7.1 software. During the calculations, SGTE 2014 database was selected to detect metallic liquid and solid solutions in the product. FACT Solutions database was chosen for the molten slag phase. A stoichiometric compound Mo_2NiB_2 was added to the calculations from a private database, whereas all gas and other stoichiometric solid phases were selected from the FACT Pure Substances database. It is obvious that as the ratio of the initial components changes, the product composition will be different. However, the following calculation trials were done for a better understanding of the reaction mechanisms which predict the important steps involved in the whole process.

In the first trial, 40 g of MoO_3, 40 g of NiO and 20 g of B_2O_3 were equilibrated with 0-40 g of Al. The reaction of the process was assumed as adiabatic (ΔH=0) and the initial reaction temperature was selected as 25°C. In order to avoid the complexity of the drawing, only the calculated phases in the liquid alloy, total gas and slag products, and adiabatic temperature (T_{ad}) values are shown versus Al addition in Figure 2. The chemical species formed during the process and their amounts change largely through the reduction of oxides with different amount of Al. T_{ad} of the process increases with increasing Al addition due to the exothermic nature of the SHS reactions. At low Al

Table 4: FactSage calculated compositions and T_{ad} values, and actual elemental compositions of the as-cast alloys from the second series of experiments.

No	wt%								
	FactSage Calculated Compositions				Actual Compositions				
	Mo	Ni	B	Al	Mo	Ni	B	Al	T_{ad}(°C)
D	55.15	38.22	5.57	1.05	50.2	42.6	3.28	3.02	2512
E	47.24	46.04	5.42	1.30	43.08	49.27	3.3	2.3	2381
F	34.0	59.71	5.51	0.78	35.51	57.59	4.1	2.2	2233

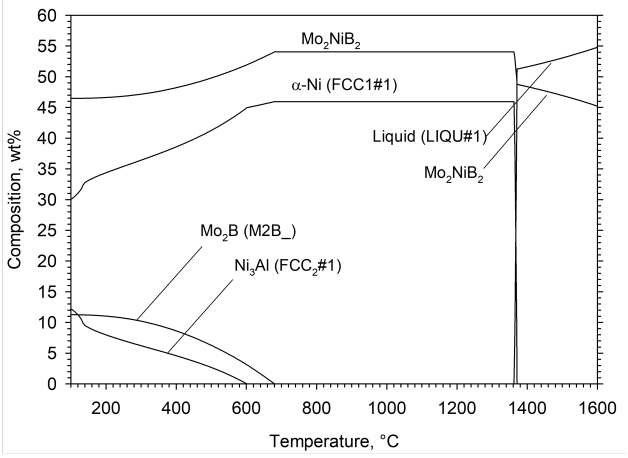

Figure 3: FactSage calculation of a selected SHS alloy for equilibrium solidification (50% Ni, 44% Mo, 4% B, and 2 wt% Al, by mass)

additions and T_{ad} values, B_2O_3 first reacts with Al_2O_3 and forms a slag phase. As seen in the figure, having more than a certain level of boron (>~3 wt%) in the alloy requires a high amount of Al, which results in a higher T_{ad} value (> 2400°C) with a dissolution of Al in the as-cast alloy. Since NiO reduction to metallic nickel generates a high amount of heat, dominant species in the initial gaseous phase (between 8-20 g Al) are mainly composed of Mo_2O_6, Mo_3O_9 and Mo_4O_{12} due to the evaporation of some MoO_3. After a certain amount of Al (>20 g Al), the simultaneous reductions of NiO and MoO_3 stimulate the release of gaseous boron oxide products such as $(BO)_2$, B_2O_3, and $AlBO_2$. The equilibrium conditions were assumed in a closed system at 1 atm in the simulation. So, it is possible to reduce almost all gaseous molybdenum species and some boron oxide particles in the closed system to the alloy phase. In the experiments, however, the cover of the copper reactor vessel was not sealed enough to prevent gas leakage (*i.e.* the molybdenum and boron oxide species) which resulted in a certain decrease in the alloy recovery.

It was also revealed that even when the stoichiometric amount of Al (~40 g) was used to attempt to reduce all oxides in the mixture, a considerable amount of Al (5.4 wt% Al) dissolved in the alloy product with a high T_{ad} value (~2620°C).

The second trial of the calculation was done for predicting the solidification of an SHS produced alloy melt to estimate the possible microstructures. For this aim, the alloy composition consisting of 50 wt% Ni, 44 wt% Mo, 4 wt% B, and 2 wt% Al by mass was selected for the equilibrium solidification model starting from 1600°C down to 100°C. Figure 3 shows that Mo_2NiB_2 is the first solid product in the liquid alloy. The solid solution α-Ni and Mo_2NiB_2 phases coexist below solidus temperature (1360°C). The calculation suggests that the nucleation of Mo_2B and Ni_3Al phases begin at 680°C and 601°C, respectively. The nickel and molybdenum to form Ni_3Al and Mo_2B phases are supplied from α-Ni and Mo_2NiB_2 phases. The subsequent calculations revealed the possibility of MoB and Ni_3B phases depending on Mo/Ni ratio in the alloy. It is noted that Al concentration in the alloy is also an important parameter for the phase formations. For example, the excess aluminum in the initial SHS mixture may lead to some other possible intermetallics in the alloy such as Ni_5Al_3, NiAl, and Ni_2Al_3.

On the basis of above FactSage results, in order to decrease the aluminum concentration in the alloy, the aluminum in the initial mixture has to be less than stoichiometric amount required for the full reduction from the oxides. Thus, in the second series of experiments, a relatively higher amount of B_2O_3 was used to depress the T_{ad} value releasing higher amounts of boron containing gases. The compositions of the initial mixtures determined by using FactSage program to obtain the as-cast alloys with high Mo_2NiB_2 and with low Al concentrations are shown in Table 1. The FactSage calculated compositions and T_{ad} values and chemical analysis results of the product samples from the second series of experiments obtained by AAS are shown in Table 4. The actual alloy compositions were found similar to the calculated ones. T_{ad} values were relatively low and varied between 2233 and 2512°C. The Mo/Ni weight percent ratios in the samples were found to be between 1.18 and 0.62. The aluminum contents in the sam-

Table 5: The EDS measured elemental compositions for crystalline phases shown in Figures 5(b), 6(b) and 7(b).

		wt%				
	No	**Mo**	**Ni**	**B**	**Al**	**Phase**
Figure 5(b)	1	89.48	2.06	8.47		MoB
	2	75.46	17.96	6.58		Mo_2NiB_2
	3		84.34	7.18	8.47	τ-$Ni_{20.5}Al_{2.5}B_6$
	4		85.74		14.26	Y'-Ni_3Al
	5		74.06		25.94	NiAl
Figure 6(b)	1	85.29		14.71		MoB_2
	2	70.59	22.41	7.00		Mo_2NiB_2
	3		90.97	5.27	3.77	τ-$Ni_{20.5}Al_{2.5}B_6$
	4		87.1		12.9	Y'-Ni_3Al
Figure 7(b)	1	75.95	18.92	5.13		Mo_2NiB_2
	2	71.11	24.65	4.24		Mo_2NiB_2
	3		87.1		12.9	Y'-Ni_3Al
	4		92.42	3.83	3.75	τ-$Ni_{20.5}Al_{2.5}B_6$

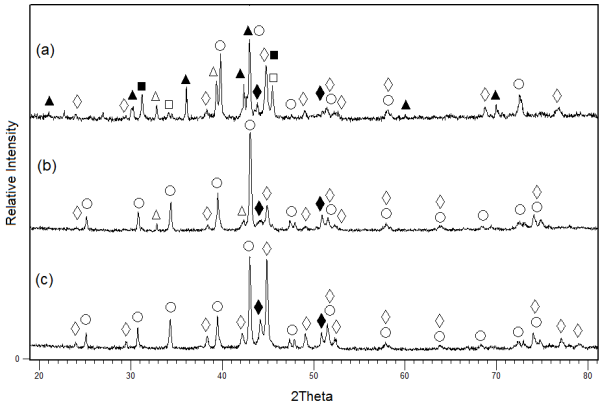

Figure 4: XRD analysis of products with compositions of a) Sample D, b) Sample E, c) Sample F (○Mo_2NiB_2, ◊ τ-$Ni_{20.5}Al_{2.5}B_6$, ♦ Y'-Ni_3Al, ■ β-NiAl, ▲ Orthorhombic α-MoB, △ Tetragonal β-MoB, □ Hexagonal MoB_2)

ples varied from 2.2 to 3.02 wt%, whereas boron contents changed between 3.3 and 4.1 wt%.

The XRD analyses of the as-cast products obtained from the second series of experiments by using the initial mixture of MoO_3: NiO: B_2O_3: Al are presented in Figure 4. Unlike the previously produced as-cast alloys, the matrix is mainly composed of τ-nickel aluminum boride (τ-$Ni_{20.5}Al_{2.5}B_6$) and Y'-nickel aluminide (Y'-Ni_3Al) phases. τ-borides with a $M_{23}C_6$-type cubic structure in ternary Ni-Al-B system have a rather broad range of homogeneity and are formed due to partial replacement of Al atoms by boron [21]. In Figure 4a, the order of the peak intensity of the phases from highest to lowest was found to be τ-$Ni_{20.5}Al_{2.5}B_6$, Y'-Ni_3Al, α and β-MoB, MoB_2, β-NiAl, and Mo_2NiB_2. Figure 4(b) shows that when the Mo/Ni weight percent ratio decreased from 1.18 to 0.87, Mo_2NiB_2 appears to be the main phase in the as-cast alloy. The second reinforcement phase detected in the alloy was α-MoB. With the further increase in Ni content from 49.27 to 57.59 wt%, MoB phase disappears and τ-$Ni_{20.5}Al_{2.5}B_6$ becomes the dominant phase in the as-cast alloy having a high Mo_2NiB_2 content (Figure 4c).

Selected SEM/BSE images of the three as-cast alloys from the second series of experiments are shown in Figures 5 to 7. Also, the elemental distributions of the phases in as-cast alloys revealed by EDS scans are listed in Table 5. Figure 5a shows the elongated particles (light gray) which are distributed throughout the matrix region (dark gray). The higher magnification SEM image in Figure 5b and the corresponding EDS analysis presented in Table 5a reveals the following phases: a) MoB (1, Whitish gray) formed in the middle of the grains b) elongated Mo_2NiB_2 particles near the boundaries (2, light gray), and the matrix c) consisting of $Ni_{20}Al_3B_6$ (3, dark gray) with mixture of Ni_3Al and NiAl (4, black dot) phases.

Figure 6a shows the plate-like particles (light gray) which are almost uniformly distributed throughout the region. The higher magnification SEM image shown in Figure 6b reveals the existence of a) plate-like Mo_2NiB_2 (1, light gray) particles , b) α-MoB (2, whitish gray) formed in the coarse Mo_2NiB_2 grains, and c) τ-$Ni_{20.5}Al_{2.5}B_6$ (3, gray) and Ni_3Al (4, dark gray) phases as the matrix.

Figure 7a shows that the plate-like particles (gray) are much longer and randomly distributed throughout the region. The higher magnification SEM image shown in Figure 7b reveals the existence of a) plate-like Mo_2NiB_2

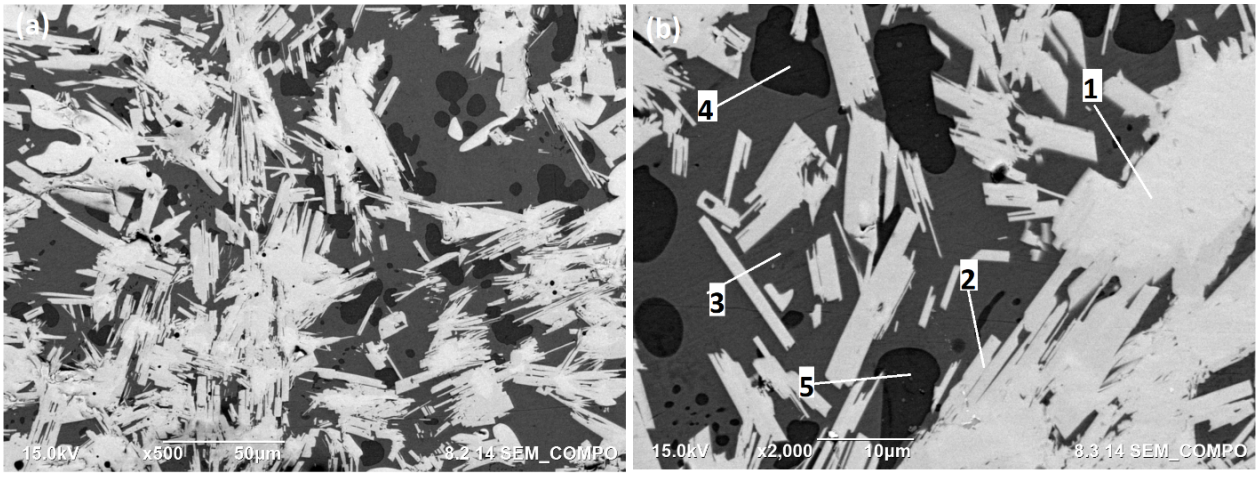

Figure 5: SEM/BSE images of the as-cast alloy sample D with the magnifications of a) ×500 and, b) ×2000

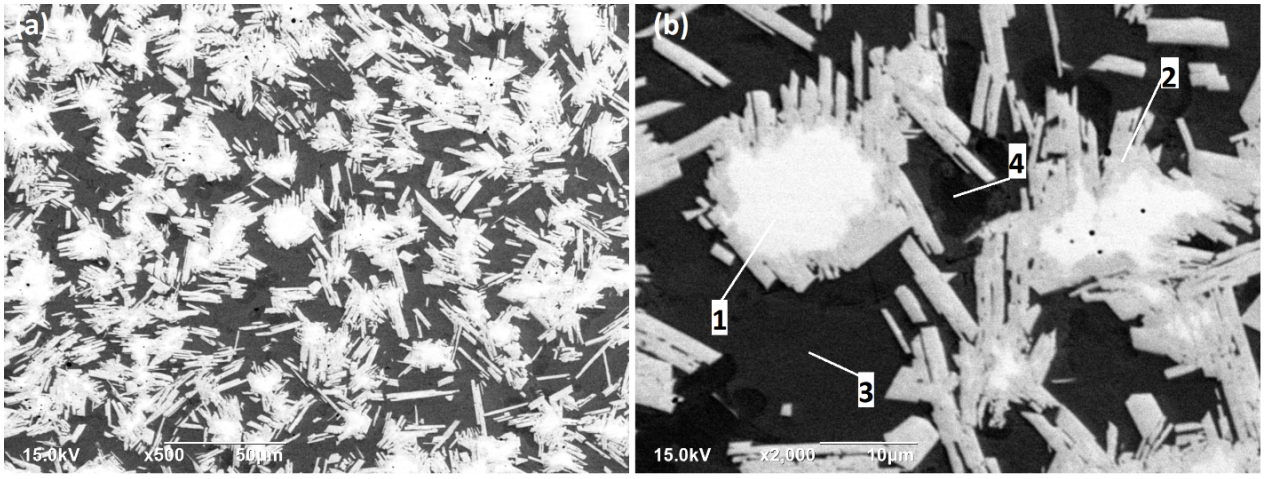

Figure 6: SEM/BSE images of the as-cast alloy sample E with the magnifications of a) ×500 and, b) ×2000

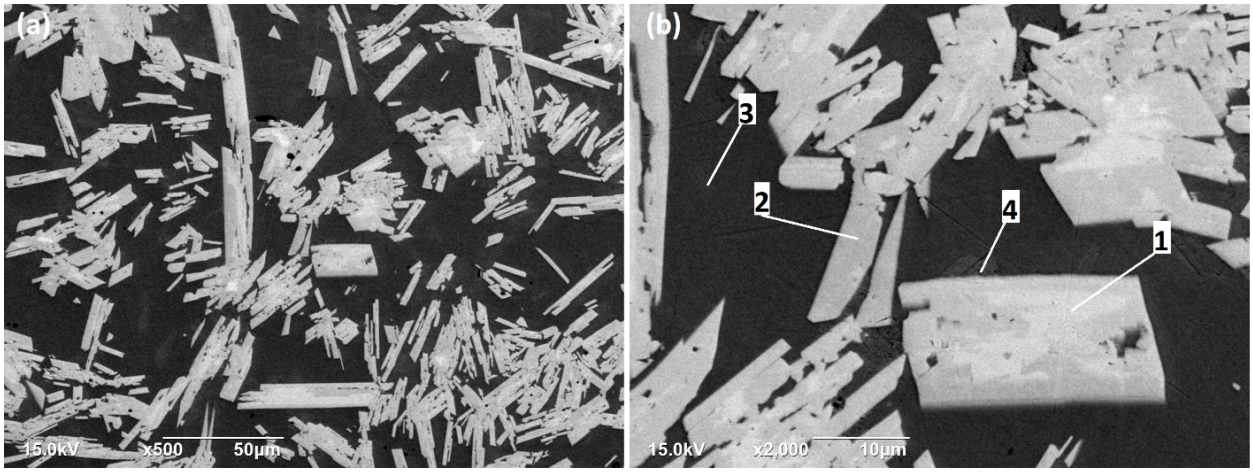

Figure 7: SEM/BSE images of the as-cast alloy sample F with the magnifications of a) ×500 and, b) ×2000

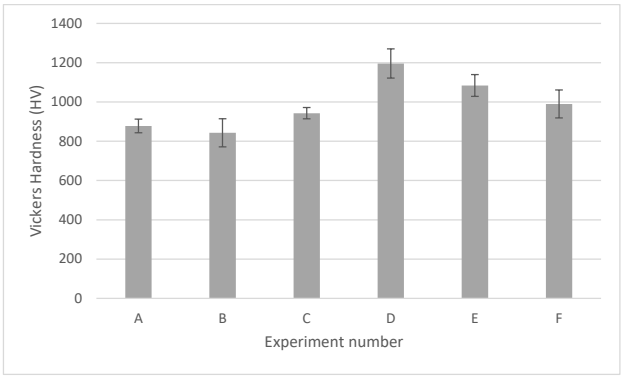

Figure 8: Variation of hardness values in products with different compositions

phases (1 and 2) with different Mo/Ni ratios, and b) Ni_3Al (3, dark gray) and τ-$Ni_{20.5}Al_{2.5}B_6$ (4, gray) phases as the matrix. The reinforcement/matrix ratios obtained from the SEM images of alloys D, E and F, were calculated to be 1.22, 1.27 and 0.72 respectively. It becomes more evident in alloy F that, as Ni forms the main matrix phases such as NiAl, Ni_3Al and $Ni_{20.5}Al_{2.5}B_6$, the reinforcement content decreased with a certain amount of Ni in the final product.

Vickers hardness measurements were performed on the Mo-Ni-B-Al hard alloys with 10 tests each and the average values are presented in Figure 8. As expected, due to the different binary or ternary matrix and reinforcements phases, as well as different reinforcement/matrix ratios, the alloys showed large deviations in the hardness values ranging from 843±71.64 HV to 1196±71.19 HV. For example, the alloys A and B showed relatively lower hardness values, since high amount of Al resulted in NiAl formation in the matrix.

The hardness value of alloy C (943 HV±28.78) slightly increased due to the relatively lower Al concentration in the matrix and higher ternary boride formation in the reinforcement phase. Sample D which has the highest hardness value (1196 HV±71.19), contains four reinforcement phases (α and β-MoB, MoB_2 and Mo_2NiB_2) and three matrix phases (τ-$Ni_{20.5}Al_{2.5}B_6$, NiAl, and Y'-Ni_3Al). As expected in alloy F, after a certain value of Ni, the hardness value decreased due to increasing matrix/reinforcement ratio in the as-cast alloys. It can be concluded that the reinforcing boride phases improved the hardness values of the composites with Ni_xAl (x=1,3) phase matrix, as also reported in the literature [22].

4 Conclusion

On the basis of the presented modeling and experimental results of the SHS process of MoO_3, NiO and B_2O_3 with Al to produce Mo_2NiB_2 containing hard materials, the following conclusions can be made: the B_2O_3 amount was used higher than its stoichiometric ratio which resulted in lower adiabatic temperature and lower Al residues in the products. Also, as the Mo/Ni weight ratio and Al content decreased, the formation feasibility of Mo_2NiB_2 ternary boride increased. Therefore, the following phases were detected in the as-cast alloys respectively: tetragonal MoB and Mo_2NiB_2 as reinforcement phases and Y'-Ni_3Al and τ-$Ni_{20.5}Al_{2.5}B_6$ as matrix phases. The average hardness values in the as-cast alloys varied between 843±71.64 HV and 1196±71.19 HV due to the compositional variations and differences in the reinforcement/matrix ratio. Further study (*i.e.* different compositions, fracture toughness, wear resistance tests, etc) is needed to properly assess the full potential of SHS produced Mo-Ni-B-Al as-cast alloys for special applications.

Acknowledgement: The authors are gratefully acknowledged for the financial support of The Scientific and Technological Research of Turkey (TUBITAK, Project No: 213M555), Istanbul Technical University Research Foundation (ITU-BAP, Project No: 39662) and Russian Foundation for Basic Research (RFBR, Project No:14-08-91374).

References

[1] V.K. Sarin, D. Mari, and L. Lianes, Comprehensive Hard Materials, Elsevier, Amsterdam, (2014).
[2] K. Takagi, W. Koike, A. Momozawa, and T. Fujima, Solid State Sci., 14 (2012) 1643-1647.
[3] W. Yongguo and L. Zhaoqian, Mater. Res. Bull., 37 (2002) 417-423.
[4] K. Takagi, J. Solid State Chem., 179 (2006) 2809-2818.
[5] K. Takagi and Y. Yamasaki, J. Solid State Chem., 154 (2000) 263-268.
[6] K. Takagi, Y. Yamasaki, and K. Hirata, Mater. Sci. Forum, 539 (2007) 803-809.
[7] Y. Yamasaki, M. Nishi, and K. Takagi, J. Solid State Chem., 177 (2004) 551-555.
[8] K. Takagi, Mater. Chem. Phys., 67 (2001) 214-219.
[9] Y. Shiota, Y. Miyajima, T. Fujima, and K. Takagi, J. Phys.: Conf. Ser. 176 (2009) 012046.
[10] K. Hirata, K. Iwanaga, Y. Yamasaki, and K. Takagi, Mater. Sci. Forum, 534 (2007) 1157-1160.
[11] S. Yazici and B. Derin, Int. J. Refract. Metals Hard Mater., 29 (2011) 90-95.

[12] T. Chanadee, J. Wannasin, and S. Niyomwas, J. Ceram. Soc. Jpn., 122 (2014) 496-501.
[13] B. Derin, U. Demircan, and O. Yucel, Met. Mater. Int., 15 (2009) 331-336.
[14] L. Guanghua, L. Jiangtao, and C. Kexin, Int. J. Refract. Metals Hard Mater., 39 (2013) 90-102
[15] A. Varma, A. S. Rogachev, A. S. Mukasyan, and S. Hwang, Advances in Chemical Engineering, Elsevier, Amsterdam, 24 (1998) pp. 79-226.
[16] E. A. Levashov, A. S. Mukasyan, A. S. Rogachev, and D. V. Shtansky, Int. Mater. Rev., 62 (2017) 203-239.
[17] V.I. Yukhvid, Pure Appl. Chem, 64 (1992) 977-988.
[18] G.F. Tavadze and A.S. Shteinberg, Production of Advanced Materials by Methods of Self-Propagating High-Temperature Synthesis, Springer, Heidelberg, (2013).
[19] V. Sanin, D. Ikornikov, D. Andreev, V. Yukhvid, B. Derin, and O. Yucel, Int. J. Self Propag. High Temp. Synth., 24 (2015) 161-170.
[20] C.W. Bale, E. Bélisle , P. Chartrand, S.A. Decterov, G. Eriksson, A.E. Gheribi, et al., CALPHAD, 54 (2016) 35-53.
[21] V. N. Sanin, D. M. Ikornikov, D. E. Andreev, V. I. Yukhvid, E. A. Levashov, and Yu.S. Pogozhev, Int. J. Self Propag. High Temp. Synth., 23 (2014) 232-239.
[22] P. Hyjek, I. Sulima, and L. Jaworska, Arch. Metall. Mater., 62 (2017) 1511-1520.